HHS Public Access

Author manuscript

Cell. Author manuscript; available in PMC 2020 June 27.

Published in final edited form as:

Cell. 2019 June 27; 178(1): 176–189.e15. doi:10.1016/j.cell.2019.05.003.

Lactate is a natural suppressor of RLR signaling by targeting MAVS

Weina Zhang[1,2,*], **Guihua Wang**[2,3,*], **Zhi-Gang Xu**[4], **Haiqing Tu**[1], **Fuqing Hu**[3], **Jiang Dai**[1], **Yan Chang**[1], **Yaqi Chen**[3], **Yanjun Lu**[3], **Haolong Zeng**[3], **Zhen Cai**[2], **Fei Han**[2], **Chuan Xu**[2], **Guoxiang Jin**[2], **Li Sun**[2], **Bo-Syong Pan**[2], **Shiue-Wei Lai**[2], **Che-Chia Hsu**[2], **Jia Xu**[4], **Zhongzhu Chen**[4], **Hong-Yu Li**[5], **Pankaj Seth**[6], **Junbo Hu**[3], **Xuemin Zhang**[1], **Huiyan Li**[1], and **Hui-Kuan Lin**[2,7,&]

[1]State Key Laboratory of Proteomics, Institute of Basic Medical Sciences, National Center of Biomedical Analysis; State Key Laboratory of Toxicology and Medical Countermeasures, Institute of Pharmacology and Toxicology, National Center of Biomedical Analysis, Beijing, Beijing 100850, China.

[2]Department of Cancer Biology, Wake Forest Baptist Medical Center, Wake Forest University, Winston Salem, NC, 27101, USA.

[3]Department of Gastrointestinal Surgery Center and Department of Laboratory Medicine, Tongji Hospital, Tongji Medical College, Huazhong University of Science and Technology, Wuhan, Hubei 430030, China.

[4]International Academy of Targeted Therapeutics and Innovation, Chongqing University of Arts and Sciences, Chongqing 402160, China.

[5]University of Arkansas for Medical Sciences, College of Pharmacy, Division of Pharmaceutical Science, 200 South Cedar, Little Rock AR 72202, USA.

[6]Division of Interdisciplinary Medicine and Biotechnology, Beth Israel Deaconess Medical Center, Harvard Medical School, Boston, MA, United States.

[7]Graduate Institute of Basic Medical Science, China Medical University, Taichung 404, Taiwan.

SUMMARY

RLR-mediated Type-I IFN production plays a pivotal role in elevating host immunity for viral clearance and cancer immune-surveillance. Here we report that glycolysis, which is inactivated

[&]Lead contact, Correspondence: hulin@wakehealth.edu.

Author contributions: W.-N.Z. and G.-H.W. designed and conducted most of the experiments. Z.-G.X., J.X., Z.-Z.C. and H.-Y.L. provided technical support, F.-Q.H, H.-Q.T carried out immunofluorescence analysis; J.D., Y.C., Y.-Q.C contributed to animal assay. Y.-J.L. and H.-L.Z. performed mass spectrometry analysis, Z.C., F.H., C.X., G.-X.J., L.S., B.-X.P., S.-W.L. and C.-C.H. provided critical comments and suggestions; J.-B.H., X.-M.Z., H.-Y.L. provided suggestions,. P.S. provided Cre^{tm}-LDHA$^{fl/fl}$ mice. W.-N.Z., G.-H.W. and H.-K. L analyzed the data and wrote the manuscript.

[*]These two authors contribute equally to this work

Declaration of Interests: The authors declare no competing interests.

during RLR activation, serves as a barrier to impede type-I IFN production upon RLR activation. RLR-triggered MAVS-RIG-I recognition hijacks hexokinase binding to MAVS, leading to the impairment of hexokinase mitochondria localization and activation. Lactate serves as a key metabolite responsible for glycolysis-mediated RLR signaling inhibition by directly binding to MAVS transmembrane (TM) domain and preventing MAVS aggregation. Notably, lactate restoration reverses increased IFN production caused by lactate deficiency. Using pharmacological and genetic approaches, we show that lactate reduction by LDHA inactivation heightens type-I IFN production to protect mice from viral infection. Our study establishes a critical role of glycolysis-derived lactate in limiting RLR signaling and identifies MAVS as a direct sensor of lactate, which functions to connect energy metabolism and innate immunity.

Graphical Abstract

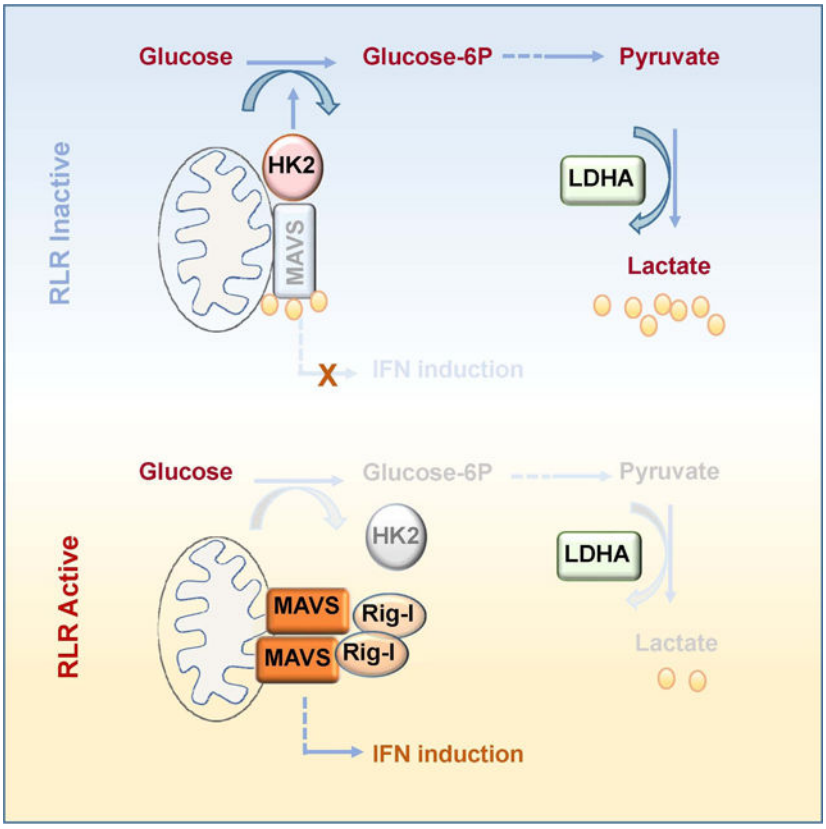

eTOC

Lactate acts as a regulator of the adaptor MAVS, allowing a cross-regulation between antiviral signaling and energy metabolism

INTRODUCTION

Type-I interferons (IFNs) produced by almost all type of cells play a vital role in host defense against viral infection and cancer immunosurveillance (Ivashkiv and Donlin, 2014; Zitvogel et al., 2015). Type-I IFNs composed of IFNα, IFNβ and other IFNs are induced

following activation of cell-surface or intracellular pattern recognition receptors (PRRs), including retinoic acid-inducible gene I (RIG-I) like receptors (RLRs), stimulator of IFN genes protein (STING) and Toll-like receptors (TLRs) (Burdette et al., 2011; Kawai and Akira, 2010; Trinchieri, 2010). In response to microbial products (e.g. viral or bacterial components) or endogenous molecules (e.g. cytosolic and extracellular DNA and RNA), PRRs transmit distinct downstream signaling pathways to trigger type-I IFN production. Upon recognized by IFN receptors, type-I IFN signal activates the Janus kinase (JAK) signal transducer and activator of transcription (STAT) pathway, leading to the expression of IFN-stimulated genes (ISGs), which control innate and adaptive immunity and intracellular antimicrobial programs (MacMicking, 2012; Schoggins et al., 2011; Stark and Darnell, 2012).

RLRs like RIG-I and MDA5, as members of PRRs, are main cytosolic RNA sensors to trigger innate immune response by sequentially activating downstream axis for type-I IFN production (Schlee and Hartmann, 2016; Seth et al., 2005). Upon sensing diverse cytosolic dsRNAs, RIG-I undergoes conformational changes, oligomerization and exposure of the N-terminal CARD domains to recruit a signaling adaptor called mitochondrial antiviral-signaling protein (MAVS). The transmembrane domain (TM domain) at C-terminus of MAVS is necessary for its mitochondrial outer membrane localization. Once activated, MAVS develops a functional prion-like structure at mitochondria, which serves as a platform to form a MAVS signalosome for activating TBK1 and IKKe. Phosphorylation of IRF3 and NF-kB by TBK1 and IKKe drives their nuclear translocation, leading to subsequent transcription of type-I IFN and inflammatory cytokine (Honda et al., 2006; Hou et al., 2011; Ivashkiv and Donlin, 2014; Tamura et al., 2008). Although intracellular RLR-MAVS activation and type-I IFN induction are orchestrated by numerous mechanisms (Chen et al., 2013a; Feng et al., 2017; Gack et al., 2007; Jin et al., 2017; You et al., 2013; Zhu et al., 2014), little is known about whether energy metabolism, likely through the production of a certain metabolite, is crucially involved in the regulation of this key signaling node allowing for the host defense against virus.

As a major source of cellular energy and cell mass, glucose is metabolized via glycolysis into pyruvate, which can either be imported to mitochondria for tricarboxylic acid (TCA) cycle entry to generate acetyl-CoA, through pyruvate dehydrogenase complex (PDHc) in the presence of oxygen, or be catalyzed by lactate dehydrogenase (LDH) to generate lactate when oxygen is not available. Interestingly, most cancer cells are addicted to aerobic glycolysis known as “Warburg effect” for their survival and proliferation even in the presence of oxygen, accompanied by high lactate generation (DeBerardinis and Thompson, 2012; Parks et al., 2013). Although lactate is previously considered as a waste-product of glucose metabolism, accumulating evidence has underscored its pivotal role in regulating diverse biological processes, such as macrophage polarization, T helper cell differentiation as well as tumor immune-surveillance (Brand et al., 2016; Colegio et al., 2014; Peng et al., 2016). Till now, no direct protein target of lactate is identified to our knowledge. Whether lactate participates in other intracellular signal transduction and biological outcome through direct protein targeting remains to be determined.

RESULTS

Downregulation of glucose metabolism promotes RLR induced type-I IFN production.

To investigate whether energy metabolism participates in regulating type-I IFN production, we employed an unbiased, systemic metabolomics approach to examine the global metabolic changes during RLR-induced type I IFN production. Intriguingly, most metabolic intermediates downstream of glucose, such as phosphoenolpyruvate (PEP), pyruvate and lactate, exhibited decreased levels at the initial stage of type I IFN production (Figure 1A and 1B). The levels of TCA intermediates, such as aconitate, succinate, fumaric acid and malate, were also significantly downregulated, likely resulting from the reduced level of pyruvate, which shunts into the TCA cycle for the production of these intermediates. However, oxaloacetate (OAA) level was not significantly affected (Figure 1A). As the direct pyruvate downstream metabolite, Acetyl-CoA production would be expected to decrease due to the reduction in pyruvate level, leading to the slower consumption of OAA for citrate production and thus maintaining the OAA level. These results suggest that glucose metabolism is impaired during the RLR signaling activation.

Systemic glucose metabolism changes during RLR-induced type-I IFN production raised the possibility that glucose catabolism is involved in the regulation of type-I IFN production. To test this possibility, we incubated cells with high or low glucose to monitor RLR induced cytokine production and found low glucose-treated cells showed much stronger induction of IFN-β and IL-6 mRNA upon poly(I:C) transfection, but not HTDNA or LPS treatment, which activates stimulator of interferon genes (STING) and Toll-like receptor (TLR) signaling, respectively, compared with those under high glucose treatment (Figure 1C–1E and Figure S1A–S1D), indicative of the specificity of glucose change in regulating RLR signaling. Importantly, higher IFN-β induction and lower virus replication were observed in fasted mice treated with low glucose compared to those treated with high glucose (Figure 1F and 1G). Similarly, 2-deoxy-glucose (2-DG), which blocks glucose metabolism by inhibiting hexokinase (HK) activity, markedly enhanced IFN-β and IL-6 production driven by different RLR stimuli including poly(I:C) transfection, Sendai virus (SEV) and Vesicular stomatitis virus (VSV) infection, leading to the reduction in virus replication (Figure 1H–1J and Figure S1E–S1G). These data suggest that downregulation of glucose metabolism promotes RLR induced type-I IFN production.

Mitochondria hexokinase activity is maintained by MAVS and inactivated during RLR activation.

Since most glucose intermediates downstream of hexokinase (HK) were down-regulated during RLR-mediated type-I IFN induction (Figure 2A), it is conceivable that HK activity might be affected during RLR activation. Indeed, HK activity decreased at early phase of RLR activation, correlated well with dynamic changes of glucose metabolites (Figure 2B and Figure S2A), indicating that a transient suppression of glucose metabolism through HK inhibition may be required for RLR-mediated type-I IFN induction. To further validate our notion, we knocked down HK2, the major isoform of HK in most human cell types, to mimic the suppression of glucose metabolism. Consistently, HK2 knockdown not only decreased glycolysis determined by reduced pyruvate and lactate levels, but also markedly

enhanced TBK1-IRF3 signaling, cytokine production and SEV replication suppression upon RLR activation (Figure 2C and Figures S2B–S2E). Moreover, restoration of HK2 expression compromised the heightened effect of HK2 knockdown on IFN-β induction (Figures S2F).

The mitochondria localization of HK2 is required for its activation and full glycolytic function in cell (DeWaal et al., 2018; Roberts and Miyamoto, 2015; Wolf et al., 2016). To gain insight into how HK activity was downregulated at early stage of RLR activation, we examined whether mitochondria HK2 level changes upon RLR activation. Of note, mitochondria HK2 decreased upon the Poly(I:C) transfection, but not HTDNA or LPS treatment (Figure 2D), which might account for the downregulation of HK activity during RLR activation. We next explored the mechanism underlying HK2 dissociation from mitochondria. Interestingly, MAVS, as a mitochondria localized protein, physiologically interacted with HK2, but not with other mitochondria proteins, like Tom20 (Figure 2E). Remarkably, the interaction between MAVS and HK2 declined during initial activation of RLR signaling triggered by Sev infection, but not STING signaling activation upon HTDNA transfection, correlated with the dissociation of HK2 from mitochondria (Figure 2F and Figure S2G). Moreover, a direct switch of MAVS binding from HK2 to RIG-I was observed in cells with ectopic expression of activated form of RIG-I (Figure 2G and Figure S2H). Furthermore, the dissociation of HK2 from MAVS upon RLR activation was not observed in RIG-I knockdown cells (Figure 2H and Figure S2I). These results suggested that RLR-triggered MAVS-RIG-I recognition hijacks HK2 binding to MAVS, leading to the impairment of HK mitochondria localization and activation.

As the downregulation of HK activity during RLR activation coincidences with RIG-I-MAVS recognition and subsequent MAVS activation upon RLR agonist stimulation (Schlee and Hartmann, 2016; Seth et al., 2005), we asked whether MAVS can regulate mitochondria HK activity. Interestingly, we found significant reduction of HK activity was observed in MAVS knockdown and knockout cells compared to control cells, accompanied by decreased pyruvate and lactate levels as well as extracellular acidification rate (ECAR) (Figure 2I-2J and Figure S2J–2K). These result suggest that MAVS maintains HK activity.

HK associates with the mitochondrial outer membrane through its interaction with the voltage-dependent anion channel (VDAC), which is involved in glycolysis regulation (Roberts and Miyamoto, 2015; Wolf et al., 2016). To examine whether VDAC binding to HK2 is necessary for the interaction between HK2 and MAVS, we applied a peptide that is known to disrupt HKs from VDAC (Prezma et al., 2013). Notably, disrupting VDAC1 and HK2 interaction by this peptide impaired the interaction of MAVS with HK2, indicating that binding to VDAC is required for HK2 interaction with MAVS (Figure S2L and S2M). Collectively, we conclude that MAVS is a previously unrecognized key regulator for HK, and switching MAVS binding from HK2 to RIG-I during RLR activation triggers HK2 release from mitochondria leading to impairing HK activity and subsequent glucose metabolism.

Anaerobic glycolysis inhibits RLR triggered MAVS-TBK1-IRF3 activation and type-I IFN production.

As the two major glucose catabolism pathways, oxidative phosphorylation (OXPHOS) and anaerobic glycolysis are tightly controlled in cells by a multistep mechanism to execute diverse biological processes (Lunt and Vander Heiden, 2011). We showed that downregulation of glucose metabolism is required for full activation of RLR signaling. To dissect the key step of glucose metabolism involved in regulating type-I IFN production, we adapted various strategies to challenge glucose metabolism either by triggering the switch from OXPHOS to anaerobic glycolysis or vice versa. Metabolic fate of pyruvate is mainly controlled by LDHA and PDHc, which convert pyruvate to lactate or acetyl-CoA for TCA cycle, respectively (Ganeshan and Chawla, 2014). As the crucial PDHc subunit, PDHA knockdown impaired mitochondria OXPHOS, thus promoting anaerobic glycolysis for lactate production. Interestingly, we found robust decrease of IFN-β production in PDHA knockdown cells compared with control cells upon RLR activation (Figure 3A and Figure S3A–S3D). Similarly, the treatment of cells with UK5099, a potent inhibitor of the mitochondria pyruvate transporter blocking pyruvate mitochondria entry for OXPHOS (Davies et al., 2017; Liu et al., 2018), elevated lactate level and led to decreased MAVS signaling and IFN-β induction (Figure S3E–S3H). By contrast, dichloroacetate (DCA), which shifts glucose metabolism from anaerobic glycolysis to OXPHOS by inhibiting pyruvate dehydrogenase kinase and thus activating PDHc (Baker et al., 2000; Michelakis et al., 2008), promoted IFN-β induction upon RLR activation, accompanied by the reduction of lactate level (Figure 3B and Figure S3I). Cells grown in galactose conditions are forced to respire by using OXPHOS instead of anaerobic glycolysis (Chang et al., 2013; Rossignol et al., 2004; Weinberg et al., 2010). While galactose expectedly impaired anaerobic glycolysis-mediated lactate production, it markedly enhanced IFN-β and IL-6 production upon poly(I:C) or Sev challenge (Figure 3C and Figure S3J–S3L). As a result, cells infected with GFP-labeled VSV showed a marked reduction in viral replication, as determined by GFP fluorescence, under galactose treatment (Figure 3D). These data suggest that anaerobic glycolysis serves as a negative signal to repress RLR-mediated MAVS signaling and cytokine production.

To further investigate the biological role of anaerobic glycolysis in RLR signaling activation, we treated cells with hypoxia, which physiologically promotes anaerobic glycolysis. While hypoxia challenge expectedly induced the expression of HIF1a targeted genes, such as VEGF and GLUT4, and promoted lactate generation, it markedly reduced IFN-β production upon RLR activation (Figure 3E and Figure S3M–S3P). Upon recognition of cytosolic RNA, RLR undergoes an ATP-dependent conformational change that facilitates MAVS oligomerization, which triggers TBK1 activation and subsequent IRF3 phosphorylation for IFN-β production. To understand how anaerobic glycolysis regulates type-I IFN production during RLR activation, we examined the phosphorylation of TBK1 and IRF3. Consistent with decreased IFN-β expression, the levels of TBK1 and IRF3 phosphorylation robustly declined in PDHA knockdown cells in response to poly(I:C) transfection (Figure 3F). Moreover, we demonstrated that PDHA knockdown attenuated MAVS aggregation upon Sev infection (Figure 3G). Taken together, these data suggest that anaerobic glycolysis suppresses RLR induced downstream activation by affecting MAVS or upstream function.

LDHA associated lactate negatively regulates RLR signaling.

Since LDHA catalyzing lactate generation from pyruvate is a key event for anaerobic glycolysis, we asked whether LDHA-associated lactate plays a role in negatively regulating type-I IFN by applying genetic and pharmacologic approaches. Indeed, knockdown of LDHA enhanced phosphorylation of TBK1 and IRF3 as well as IFN-β production upon RLR activation (Figure 4A–4C, Figure S4A and S4B). Importantly, LDHA restoration in these knockdown cells reversed this effect (Figure 4D). Similar to LDHA knockdown, treatment of sodium oxamate, a specific LDHA inhibitor (Crane et al., 2014; Zhao et al., 2014; Zhao et al., 2016), reduced lactate level and enhanced IFN-β production resulting in suppressing virus replication (Figure 4E–4H, Figure S4C and S4D). Sodium oxamate also promoted IRF3 and TBK1 phosphorylation and MAVS aggregation upon RLR activation (Figure S4E and S4F). Of note, the effect of LDHA inhibition on RLR signaling was not observed in cells treated by STING agonist (Figure S4G and S4H). Collectively, these results indicate that LDHA plays a crucial role in specifically suppressing RLR-MAVS signaling and subsequent type-I IFN production.

We next explored whether LDHA-associated lactate is a direct metabolite meditating the inhibition of RLR signaling caused by anaerobic glycolysis. Of note, addition of lactate into cells pretreated with sodium oxamate reversed the effect of LDHA inhibitor on IFN-β promotion (Figure 4I and Figure S5A). Lactate add-back also compromised the effects of 2-DG on IFN-β induction and its upstream signaling (Figure 4J and Figure S5B). Similar results were also observed in HK2 knockdown cells (Figure 4K). Moreover, we showed that add-back of lactate rescued the effects of galactose on IFN-β induction and virus replication (Figure 4L and Figure S5C). To determine how much lactate is needed to inhibit IFN production, we added back various concentrations of exogenous lactate (0–10 mM) into cells treated with galactose, and found 5 mM lactate was required for inhibiting IFN-β production (Figure 4M and Figure S5D–S5E). To rule out the possibility that lactate affects IFN-β production by changing the acidity of the medium, acidic pH of medium was adjusted to equal level as cells without addition of lactate by using NaOH before Poly(I:C) transfection. Lactate could still inhibit IFN-β production to the similar extent as the condition where PH was not adjusted (Figure S5F and S5G). As cells utilize monocarboxylate transporter 1 (MCT1) for lactate uptake, we knocked down MCT1 in cells to determine whether lactate uptake is crucial for its effect. LDHA inhibitor-Oxamate or 2-DG treatment promoted IFN-β expression, but such effect was markedly impaired upon MCT1 knockdown (Figure 4N and Figure S5H–S5I), indicating that lactate transporting into cells is essential for inhibiting MAVS signaling. Collectively, we conclude that lactate serves as a key metabolite to mediate the inhibitory effect of anaerobic glycolysis on RLR signaling.

LDHA-associated lactate inhibits RLR signaling *in vivo*.

To further confirm glycolysis-derived lactate serves as a natural suppressor of RLR induced type-I IFN production *in vivo*, mice were fasted overnight to reduce the basal glucose and lactate level and then treated with high glucose or low glucose in the presence or absence of lactate addition. While the reduction of glucose level in mice enhanced type-I IFN and IL-6 induction triggered by VSV infection, lactate add-back reversed this effect (Figure 5A and

Figure S6A), indicating that lactate plays a critical role in suppressing RLR signaling *in vivo*. Moreover, we used tamoxifen inducible LDHA knockout mice and primary macrophage cells, in which LDHA exon2 is flanked by loxP sites (Xie et al., 2014) and lactate generation is genetically inhibited, to monitor RLR-mediated cytokine production (Figure S6B). LDHA protein expression in diverse organs of $Ldha^{-/-}$ mice was abrogated upon tamoxifen treatment (Figure S6C). When challenged with VSV, $Ldha^{-/-}$ mice showed much higher cytokine induction in serum or tissue compared to that in $Ldha^{+/+}$ mice (Figure 5B–5C and Figure S6D). Consistent with elevated IFN-β level, virus replication as determined by VSV-specific mRNA in different tissues was much lower in $Ldha^{-/-}$ mice than $Ldha^{+/+}$ mice (Figure 5D). Pathological staining showed reduced infiltration of inflammatory cells in the lung of $Ldha^{-/-}$ mice compared with $Ldha^{+/+}$ mice upon VSV infection (Figure 5E). In addition, peritoneal macrophages isolated from $Ldha^{-/-}$ mice exhibited reduced lactate secretion, but elevated IFN-β induction compared with those from $Ldha^{+/+}$ mice upon poly (I:C) transfection, Sev or VSV infection, whereas no difference was observed between the groups when treated by HTDNA or HSV(Figure 5F–5G and Figure S6E–S6F). Moreover, lactate addition in $Ldha^{-/-}$ macrophage consistently reduced IFN-β production (Figure 5H). These data define the critical role of LDHA-associated lactate in suppressing RLR-mediated type-I IFN production for the host defense against viral infection *in vivo*.

Pharmacologically targeting LDHA-associated lactate enhances type-I IFN production and viral clearance *in vivo*.

Having shown that LDHA-mediated lactate serves as a nature inhibitor of RLR-mediated type-I IFN production and viral clearance *in vivo*, we then determined whether pharmacologically targeting LDHA by the LDHA inhibitor, sodium oxamate, in mice is an effective strategy to bolster IFN production for the host to defend against viral infection (Figure S6G). Remarkably, administration of sodium oxamate to mice reduced lactate production and promoted the induction of type-I IFN, IL-6 and virus clearance in various tissue samples after VSV infection (Figure 5I and Figure S6H–S6L). The effect of lactate on IFN production *in vivo* is specific for RLR, because no difference in IFN production was observed in mice injected with HSV that activates STING signaling (Figure 5J and Figure S6M). Thus, our results provide the proof of principle evidence that pharmacologically targeting LDHA by sodium oxamate is an effective strategy to enhance RLR triggered type-I IFN production for viral clearance.

LDHA-associated lactate negatively regulates RLR activation by targeting MAVS.

We next sought to identify the direct targets of lactate responsible for its action on RLR-signaling. To this end, we synthesized biotin-labeled lactate and performed biotin pulldown assay by mixing biotin-labeled lactate with the whole cell extracts. We focused on the key proteins that are involved in cytosolic RLR signaling activation including RIG-I, MDA5, TBK1, MAVS and IRF3 and found lactate specifically interacted with MAVS, but not with other components of cytosolic RLR signaling or other mitochondria proteins such as Tom20 (Figure 6A), indicative of the specificity of this interaction. Mass spectrometry analysis also identified a cluster of MAVS peptides in the lactate pulldown complex (Figure S7A). Of note, MAVS interacted with lactate, but not pyruvate, in cells under physiological conditions

(Figure 6B and 6C). By using *in vitro* binding assay, we found MAVS binds to lactate in a dose-dependent manner. Pre-incubation with excessive lactate significantly attenuated the binding of MAVS to Biotin-lactate (Figure S7B and S7C). Collectively, these data suggest that lactate directly binds to MAVS.

To explore the detailed interaction between lactate and MAVS, we carried out the domain mapping assay and found the transmembrane (TM) domain of MAVS that targets MAVS to the mitochondrial membrane is required for lactate-MAVS binding (Figure 6D and 6E). We next synthesized a peptide that constitutes MAVS TM domain (514–535aa) or control sequence with a trans-activator of transcription (TAT) tag placed in its N terminal region (Figure 6F and Figure S7D–S7E). In an *in vitro* binding assay, we found that TM peptide markedly interrupted the binding of lactate to MAVS in dose-dependent manner (Figure 6G and Figure S7F), indicating this peptide could compete with MAVS from binding to lactate. We next examined whether lactate could directly bind to TM domain of MAVS. In support of this notion, mass spectrometry analysis of *in vitro* biotin-lactate pulldown products revealed that the TM peptide of MAVS, but not control peptide, could bind to biotin-lactate (Figure 6H). Furthermore, we also used Tat antibody to perform immunoprecipitation assay and found that lactate could be specifically pulled down by Tat-TM peptide in a dose-dependent manner (Figure 6I). Thus, our data demonstrate that lactate binds to TM domain of MAVS.

We took the advantage of the cell penetration property (CPP) of the TAT peptide derived from the trans-activator of transcription of human immunodeficiency virus (Milletti, 2012). This CPP has been used to deliver large molecules or even small particles into the cells for testing their biological functions by overcoming the lipophilic barrier of the cell membranes. Using the immunofluorescence assay, we found both control and TM peptide could get into cells (Figure 6J). We then determined the effect of TM peptide on RLR induced type-I IFN production. Of note, adding TM peptide to the cells promoted RLR activation in a dose dependent fashion (Figure 6K and Figures S7G–S7H). Moreover, TM peptide also compromised the inhibitory effect of lactate on IFN-β and IL-6 production upon Poly (I:C) treatment (Figure 6L and Figures S7I–S7J). Collectively, these results suggest that lactate inhibits RLR signaling through its binding to the TM domain of MAVS.

Lactate inhibits MAVS mitochondria localization, RIG-I/MAVS association and MAVS aggregation.

In order to unravel the underlying mechanism by which lactate inhibits RIG-I-MAVS induced RLR activation, we explored whether lactate impacts the mitochondria localization of MAVS by binding to its TM domain, (Seth et al., 2005). Inhibition of lactate generation by oxamate potentiated MAVS mitochondria localization, but lactate add-back compromised this effect (Figure 7A and 7B). Mitochondria localization of MAVS provides the structural basis for RIG-I-MAVS recognition and subsequent MAVS activation. We sought to determine whether activated RIG-I could still bind to MAVS devoid of TM domain of MAVS. As expected, MAVS mutant defective of TM domain which could not localize in mitochondria failed to interact with activated RIG-I (Figures 7C). Notably, LDHA inhibitor treatment enhanced the interaction between activated RIG-I and MAVS in both basal and

Sendai virus-infected conditions, whereas lactate treatment markedly reduced their binding (Figures 7D and 7E). Thus, lactate disrupts MAVS mitochondria localization and the interaction between RIG-I-MAVS interaction.

Recognition of MAVS by activated RIG-I is essential for MAVS aggregation and its downstream activation, we tested whether lactate could directly affect MAVS aggregation induced by activated RIG-I through performing *in vitro* MAVS aggregation assay. To this end, we incubated lactate with activated RIG-I protein (RIG-I(N)) along with mitochondria and ubiquitin chains as previously described (Hou et al., 2011). In the presence of mitochondria and unanchored K63-linked ubiquitin chains (K63-Ub4), we found that purified GST-RIG-I(N) triggered robust MAVS aggregation in vitro. Remarkably, lactate, but not pyruvate, impaired MAVS aggregation in a dose dependent manner (Figure 7F), indicative of direct effect of lactate on RIG-I-mediated MAVS aggregation. Collectively, these data suggest that lactate targets the TM domain of MAVS to obstruct its mitochondria localization and RIG-I-MAVS complex formation, thereby impairing MAVS aggregation and its downstream signaling activation.

DISCUSSION

Substantial evidence accumulated in recent years has highlighted the role of lactate not only in regulating tumor microenvironment and immune cell functions (Brand et al., 2016; Colegio et al., 2014), but also serving as a fuel for TCA cycle in cancer cells (Faubert et al., 2017). However, no direct targeting protein of lactate has been identified so far to help explain its mode of action. Our study identifies MAVS as a lactate sensor whose inactivation by direct lactate binding serves as a natural barrier to limit RLR signaling activation for type-I IFN production. We demonstrate that the binding of MAVS to lactate interrupts MAVS mitochondria localization, RIG-I and MAVS interaction and subsequent MAVS aggregation, thereby attenuating RLR signaling and downstream type-I IFN production (Fig. 7G).

Although metabolism has been linked to diverse biological processes, the connection between glucose metabolism and RLR-mediated innate immune activation remains puzzling. Through systematic approaches in conjunction with various biochemical assays, we unraveled that anaerobic glycolysis acts as a natural barrier to impede RLR signaling activation. Importantly, we demonstrated that glycolysis-derived lactate represents the first metabolite that directly binds to MAVS and suppresses its functions to orchestrate type-I IFN production. We rationalize that lactate accumulation by elevated LDH and/or glycolysis may be a potential mechanism for virus to evade host defense by inhibiting RLR-induced type-I IFN production. Notably, clinical studies reveal that elevated LDH or lactate levels are detected in patients under certain viral infection, especially in those with poor prognosis (Chen et al., 2013b; Hunt et al., 2015). Hence, pharmacologically targeting LDHA-dependent lactate production is a promising strategy to strengthen host innate immune response through heightening type-I IFN production for viral clearance and cancer immune-surveillance.

TM domain of MAVS is not only crucial for the mitochondria localization of MAVS, but also required for RIG-I recognition. Interestingly, our findings that TM peptide competes with MAVS from binding to lactate and lactate directly binds to TM domain of MAVS may provide the molecular basis of how lactate disrupts MAVS mitochondria localization and MAVS-RIG-I interaction, thereby impairing MAVS aggregation and RLR-mediated IFN production for viral clearance. Of note, applying TM peptide from MAVS to the cells not only enhances IFN production under normal conditions, but also relieves the inhibitory effect of lactate on RLR-mediated IFN production. Thus, our findings suggest that targeting lactate-MAVS interaction may represent another promising strategy for clinical drug development based on the knowledge learned from TM peptide to boost our body immunity for viral and cancer clearance. This strategy may offer a superior way than directly targeting LDHA, as it maintains the level of lactate for normal cellular functions.

Type-I IFNs are critical cell-intrinsic antimicrobial factors that limit the spread of infectious agents, such as viral pathogens. (MacMicking, 2012; Schoggins et al., 2011; Stark and Darnell, 2012). Beyond their important role in host defense against viruses, type-I IFNs also play a critical role in regulating the functions of diverse innate and adaptive immune cells including dendritic cell, regulatory T (TReg) cells and cytotoxic T lymphocytes (CTLs), thereby contributing to immune-surveillance of cancer (Zitvogel et al., 2015). While energy metabolism has emerged to regulate diverse biological processes, its role in RLR signaling activation and type-I IFN production has not been defined. Our study reveals that glycolysis serves as physiological barriers to limit type-I IFN production by promoting lactate generation, both *in vitro* and *in vivo*. Hence, in order to achieve optimal type-I IFN production, it is imperative for the host to develop a strategy to inactivate glycolysis and thereby reducing lactate production during RLR challenge. In this respect, we demonstrate the RLR challenge switches the recognition of MAVS from HK2 to RIG-I, resulting in HK2 mitochondria dissociation and HK inactivation. Our study therefore uncovers that MAVS is a previously unrecognized player that maintains HK2 activity and glycolysis. Thus, MAVS possess dual roles in regulating glycolysis and innate immune response, and viral infection hijacks MAVS's function from glycolysis to innate immune regulation.

Since cancer cells often overexpressed HK2 (Patra et al., 2013), exposed to hypoxia microenvironment and favored glycolysis for energy metabolism known as Warburg effect (Nakazawa et al., 2016; Pavlova and Thompson, 2016), it is likely that limiting type-I IFN production by these conditions through generating more lactate may serve as another important mechanism for cancer cells to evade immune surveillance. In summary, our study provides not only the crucial molecular insight into how energy metabolism and type-I IFN cross-talk to regulate diverse biological processes, but also offers an important paradigm and strategy for the management of various human diseases, such as viral infection and cancer.

STAR Methods

CONTACT FOR REAGENT AND RESOURCE SHARING

Further information and requests for reagents may be directed to, and will be fulfilled by the Lead Contact, Hui-Kuan Lin (hulin@wakehealth.edu).

EXPERIMENTAL MODELS AND SUBJECT DETAILS

Mice.—*Ldha*$^{+/+}$ and *Ldha*$^{-/-}$ mice on a C57BL/6J background were previously described (Xie et al., 2014). All animal procedures were approved by Institutional Animal Care and Use Committee in Wake Forest University School of Medicine. Littermates of the same sex were randomly assigned to experimental groups. 6–8 weeks old mice were treated with tamoxifen (20 mg/ml in corn oil) or coin oil by intraperitoneal injection. According to protocols provided by Jackson lab for inducible Cre driver lines, LDHA exon2 deletion was confirmed by genotyping 10 days after final injection. Mice were then used for peritonea macrophage isolation or virus infection by intraperitoneal injection. IFN-β concentration in supernatants of peritoneal macrophage or sera from *Ldha*$^{+/+}$ and *Ldha*$^{-/-}$ mice were determined by using the mouse IFN-β ELISA kit (Thermo Fisher 424001) according to the manufacturer's protocol. All the analyses were performed blindly. *Ldha*$^{-/-}$ mice were randomly allocated into experimental groups for further treatment and cell samples were allocated based on the genotype of interest.

Cells.—HEK293, Hep3B, Raw264.7 cells and immortalized bone marrow macrophage (iBMM) cells were cultured in DMEM medium supplied with 10% FBS, 2 mM glutamine, penicillin (100 U/mL) and streptomycin (100 mg/mL). THP-1 cells were cultured in RPMI-1640 medium supplied with 10% FBS, 2 mM glutamine, penicillin (100 U/mL) and streptomycin (100 mg/mL). Primary peritoneal macrophages were isolated from mice 14 days after tamoxifen intraperitoneal injection as previously described (Chen et al., 2013a). Cells were plated 24 hours before transfection with Poly(I:C) (1 μg/ml), HTDNA (1 μg/ml) or siRNA (10 nM) by Lipofectamine 2000 (Thermo Fisher Scientific). THP-1 cells were pretreated by PMA (100 ng/mL) overnight for differentiation before the next manipulation. To generate shRNA knockdown cells, HEK293T cells were prepared and co-transfected with either luciferase (shLuc) or target gene shRNA with packaging plasmid (pHelper) and envelop plasmid (pEnv) by using the calcium phosphate transfection method. Medium was changed 6 hours later and virus particles were harvested after another 48 hours to infect parental cells, then selected by puromycin.

Viruses.—VSV and HSV-1 were propagated and tittered by plague assay on Vero cells. For in vivo cytokine production studies, age and sex-matched groups of littermate mice were intraperitoneally injected with VSV or HSV-1 (2×10^7 pfu/g). For cell based assays, cells were infected with VSV-GFP (0.1 MOI) or SeV (1 MOI) for the indicated hours and cytokine production was analyzed by Q-PCR or ELISA.

METHODS DETAILS.

Immunoblotting (IB), Immunoprecipitation (IP) and Pull down assays.—For Immunoblotting, whole cell lysates were prepared in E1A buffer (50 mM Hepes, pH 7.6, 250 mM NaCl, 0.1% Nonidet P-40, 5mM EDTA) supplemented with complete protease inhibitor cocktail (Roche, 04693132001). Cell lysates were separated by SDS-PAGE and proteins were visualized by enhanced chemiluminescence according to the manufacturer's instructions (ThermoFisher Scientific). For protein-protein interactions, cells were lysed by RIPA lysis buffer (150 mM NaCl, 0.5% NP-40, 5 mM EDTA) containing a mixture of protease inhibitor cocktail (Roche). Primary antibodies were incubated with magic protein

agarose A/G beads for 30 min at room temperature, followed by incubating with cell lysates for 3 hours with rotating at RT. The beads were washed four times with lysis buffer and analyzed by IB. For Biotin-lactate pull down assays, magic Dynabeads MyOne Streptavidin T1 was preincubated with free biotin or biotin-labeled lactate in PBS for 1 hour at RT, and then incubated with cell lysates overnight with rotating at 4°C. The beads were washed 3–4 times and analyzed by Immunoblotting.

Lactate treatment.—For lactate addiction assay, we used two forms of lactate in the paper, one is the acid form of lactate (L-lactic acid), which was used for *in vitro* cell based study and *in vitro* MAVS aggregation assay, while the other one is the basic form of lactate (sodium lactate), which was used for *in vivo* animal experiments.

Immunofluorescent Confocal Microscopy.—Cells were fixed with 3% paraformaldehyde for 20 min at 25°C and permeabilized for 20 min with 0.5% Tween-20. Samples were blocked with 2% goat serum in phosphate-buffered saline (PBS) for 30 min. Anti-MAVS (1:500, Santa Cruz) and anti-TAT (1:500, Abcam) antibodies were used to detect the MAVS protein and TM peptides, respectively. Staining was visualized with secondary antibodies and the images were captured with a digital camera under a confocal microscope.

RNA extraction and quantitative RT-PCR—Total RNA was extracted via TRIzol reagent (Ambion 15596–018). Total RNAs (0.5–1mg) were subjected to reverse transcription with PrimeScript RT Master Mix (Takara, DRR036A). To determine relative mRNA level, Q-PCR was performed using universal SYBR Green Supermix (Bio-Rad 172–5125) and gene expression was normalized to that of GAPDH or HPRT. Primers used for Q-PCR were listed in Table S1.

Measurement of hexokinase activity and Lactate level.—For hexokinase activity detection, mitochondria were isolated from cells and pellet was lysed and subjected to Hexokinase activity measurement by using Hexokinase Colorimetric assay kit (Biovision K789–100). Secreted lactate level was measured by lactate Plus Test Strips (Nova Biomedical/fisher), whereas intracellular lactate level was measured by using lactate Colorimetric/Fluorometric assay kit (Biovision K607–100) according to manufacturer's protocol. For Seahorse analysis, cells with control or MAVS knockdown were prepared, the XF24 Extracellular Flux analyzer (Seahorse Biosciences, Billerica, MA) was used to measure extracellular acidification rate (ECAR).

In vivo* and *in vitro* MAVS aggregation assays.—In vivo* MAVS aggregation was performed according to published protocol (Hou et al., 2011). In brief, mitochondria were isolated by using the Mitochondria isolation kit (Thermo 89874), and mitochondria pellet was suspended in 1 × sample buffer (0.5 × TBE, 10% glycerol, 2% SDS, and 0.0025% bromophenol blue) and subjected to Semi-denaturing detergent agarose gel electrophoresis (SDD-AGE). Samples were loaded onto a vertical 1.5% agarose gel (Bio-Rad). After electrophoresis in the running buffer (1 × TBE and 0.1% SDS) for 40 min with a constant voltage of 80–100 V at 4°C, the proteins were transferred to Immobilon membrane (Millipore) for immunoblotting.

For *in vitro* MAVS aggregation, crude mitochondria were isolated and RIG-I activation was detected as previously described (Zeng et al., 2009). Briefly, each ml mixture contained 100 ng GST-RIG-I(N) and 50–100 ng ubiquitin chains (K63–Ub4 from Boston Biochem UC-310B) in buffer containing 20 mM HEPES-KOH (pH 7.0) and 10% (v/v) glycerol. After incubation at RT for 10 min in total 10 μl reaction system, 1 μl of reaction mixture was mixed with 10 μg of mitochondrial fraction in 10 μl Buffer B (20 mM HEPES-KOH [pH 7.0], 5 mM $MgCl_2$, and 0.25 M D-mannitol) at 30°C for 30 min. Mitochondria fraction was then pelleted at 10,000 g for 10 min and washed twice with Buffer C (20 mM HEPES-KOH at pH 7.4, 0.5 mM EGTA, 0.25 MD-mannitol, and EDTA-free protease inhibitor cocktail) and then subjected SDD-AGE.

QUANTIFICATION AND STATISTICAL ANALYSIS

Statistics.—Statistical significance was identified by Student's t test. p values of less than 0.05 were considered statistically significant; * $p < 0.05$, ** $p < 0.01$.

Supplementary Material

Refer to Web version on PubMed Central for supplementary material.

Acknowledgements.

We thank Drs. Zhijian Chen (UT South Western Medical Center), Qinxi Li (Xiamen University, China), Ping Gao (Xiamen University, China) and Hui Zhong (Beijing Institute of Biotechnology, China) for sharing with various plasmids. We are indebted to Dr. Steve Kridel (Wake Forest Baptist Comprehensive Cancer Center) for providing the Seahorse device for our study. We acknowledge the support of the Wake Forest Baptist Comprehensive Cancer Center Cell Engineering Shared Resource, supported by the National Cancer Institute's Cancer Center Support Grant (P30CA012197). This work is supported by Start-ups and Anderson Endowed Professorship fund from Wake Forest School of Medicine and NIH grants (R01CA182424 and R01CA193813) to H.-K.L as well as NIH grants (R01CA194094 and R01CA197178) to H.-Y.L. We also acknowledge the support by the National key research and development program (2017YFA0503900), National Natural Science Foundation of China (31671413) and Beijing Nova program (Z161100004916147) to W.-N.Z. and National Natural Science Foundation of China (81790252) to H.-Y.L.

References

Baker JC, Yan X, Peng T, Kasten S, and Roche TE (2000). Marked differences between two isoforms of human pyruvate dehydrogenase kinase. J Biol Chem 275, 15773–15781. [PubMed: 10748134]

Brand A, Singer K, Koehl GE, Kolitzus M, Schoenhammer G, Thiel A, Matos C, Bruss C, Klobuch S, Peter K, et al. (2016). LDHA-Associated Lactic Acid Production Blunts Tumor Immunosurveillance by T and NK Cells. Cell Metab 24, 657–671. [PubMed: 27641098]

Burdette DL, Monroe KM, Sotelo-Troha K, Iwig JS, Eckert B, Hyodo M, Hayakawa Y, and Vance RE (2011). STING is a direct innate immune sensor of cyclic di-GMP. Nature 478, 515–518. [PubMed: 21947006]

Chang CH, Curtis JD, Maggi LB Jr., Faubert B, Villarino AV, O'Sullivan D, Huang SC, van der Windt GJ, Blagih J, Qiu J, et al. (2013). Posttranscriptional control of T cell effector function by aerobic glycolysis. Cell 153, 1239–1251. [PubMed: 23746840]

Chen W, Han C, Xie B, Hu X, Yu Q, Shi L, Wang Q, Li D, Wang J, Zheng P, et al. (2013a). Induction of Siglec-G by RNA viruses inhibits the innate immune response by promoting RIG-I degradation. Cell 152, 467–478. [PubMed: 23374343]

Chen Y, Liang W, Yang S, Wu N, Gao H, Sheng J, Yao H, Wo J, Fang Q, Cui D, et al. (2013b). Human infections with the emerging avian influenza A H7N9 virus from wet market poultry: clinical analysis and characterisation of viral genome. Lancet 381, 1916–1925. [PubMed: 23623390]

Colegio OR, Chu NQ, Szabo AL, Chu T, Rhebergen AM, Jairam V, Cyrus N, Brokowski CE, Eisenbarth SC, Phillips GM, et al. (2014). Functional polarization of tumour-associated macrophages by tumour-derived lactic acid. Nature 513, 559–563. [PubMed: 25043024]

Crane CA, Austgen K, Haberthur K, Hofmann C, Moyes KW, Avanesyan L, Fong L, Campbell MJ, Cooper S, Oakes SA, et al. (2014). Immune evasion mediated by tumor-derived lactate dehydrogenase induction of NKG2D ligands on myeloid cells in glioblastoma patients. Proc Natl Acad Sci U S A 111, 12823–12828. [PubMed: 25136121]

Davies LC, Rice CM, Palmieri EM, Taylor PR, Kuhns DB, and McVicar DW (2017). Peritoneal tissue-resident macrophages are metabolically poised to engage microbes using tissue-niche fuels. Nat Commun 8, 2074. [PubMed: 29234000]

DeBerardinis RJ, and Thompson CB (2012). Cellular metabolism and disease: what do metabolic outliers teach us? Cell 148, 1132–1144. [PubMed: 22424225]

DeWaal D, Nogueira V, Terry AR, Patra KC, Jeon SM, Guzman G, Au J, Long CP, Antoniewicz MR, and Hay N (2018). Hexokinase-2 depletion inhibits glycolysis and induces oxidative phosphorylation in hepatocellular carcinoma and sensitizes to metformin. Nat Commun 9, 446. [PubMed: 29386513]

Faubert B, Li KY, Cai L, Hensley CT, Kim J, Zacharias LG, Yang C, Do QN, Doucette S, Burguete D, et al. (2017). Lactate Metabolism in Human Lung Tumors. Cell 171, 358–371e359. [PubMed: 28985563]

Feng H, Lenarcic EM, Yamane D, Wauthier E, Mo J, Guo H, McGivern DR, Gonzalez-Lopez O, Misumi I, Reid LM, et al. (2017). NLRX1 promotes immediate IRF1-directed antiviral responses by limiting dsRNA-activated translational inhibition mediated by PKR. Nat Immunol 18, 1299–1309. [PubMed: 28967880]

Gack MU, Shin YC, Joo CH, Urano T, Liang C, Sun L, Takeuchi O, Akira S, Chen Z, Inoue S, et al. (2007). TRIM25 RING-finger E3 ubiquitin ligase is essential for RIG-I-mediated antiviral activity. Nature 446, 916–920. [PubMed: 17392790]

Ganeshan K, and Chawla A (2014). Metabolic regulation of immune responses. Annu Rev Immunol 32, 609–634. [PubMed: 24655299]

Guan K, Zheng Z, Song T, He X, Xu C, Zhang Y, Ma S, Wang Y, Xu Q, Cao Y, et al. (2013). MAVS regulates apoptotic cell death by decreasing K48-linked ubiquitination of voltage-dependent anion channel 1. Mol Cell Biol 33, 3137–3149. [PubMed: 23754752]

Honda K, Takaoka A, and Taniguchi T (2006). Type I interferon [corrected] gene induction by the interferon regulatory factor family of transcription factors. Immunity 25, 349–360. [PubMed: 16979567]

Hou F, Sun L, Zheng H, Skaug B, Jiang QX, and Chen ZJ (2011). MAVS forms functional prion-like aggregates to activate and propagate antiviral innate immune response. Cell 146, 448–461. [PubMed: 21782231]

Hunt L, Gupta-Wright A, Simms V, Tamba F, Knott V, Tamba K, Heisenberg-Mansaray S, Tamba E, Sheriff A, Conteh S, et al. (2015). Clinical presentation, biochemical, and haematological parameters and their association with outcome in patients with Ebola virus disease: an observational cohort study. Lancet Infect Dis 15, 1292–1299. [PubMed: 26271406]

Ivashkiv LB, and Donlin LT (2014). Regulation of type I interferon responses. Nat Rev Immunol 14, 36–49. [PubMed: 24362405]

Jin S, Tian S, Luo M, Xie W, Liu T, Duan T, Wu Y, and Cui J (2017). Tetherin Suppresses Type I Interferon Signaling by Targeting MAVS for NDP52-Mediated Selective Autophagic Degradation in Human Cells. Mol Cell 68, 308–322e304. [PubMed: 28965816]

Kawai T, and Akira S (2010). The role of pattern-recognition receptors in innate immunity: update on Toll-like receptors. Nat Immunol 11, 373–384. [PubMed: 20404851]

Liu X, Cooper DE, Cluntun AA, Warmoes MO, Zhao S, Reid MA, Liu J, Lund PJ, Lopes M, Garcia BA, et al. (2018). Acetate Production from Glucose and Coupling to Mitochondrial Metabolism in Mammals. Cell 175, 502–513e513. [PubMed: 30245009]

Lunt SY, and Vander Heiden MG (2011). Aerobic glycolysis: meeting the metabolic requirements of cell proliferation. Annu Rev Cell Dev Biol 27, 441–464. [PubMed: 21985671]

MacMicking JD (2012). Interferon-inducible effector mechanisms in cell-autonomous immunity. Nat Rev Immunol 12, 367–382. [PubMed: 22531325]

Michelakis ED, Webster L, and Mackey JR (2008). Dichloroacetate (DCA) as a potential metabolic-targeting therapy for cancer. Br J Cancer 99, 989–994. [PubMed: 18766181]

Milletti F (2012). Cell-penetrating peptides: classes, origin, and current landscape. Drug Discov Today 17, 850–860. [PubMed: 22465171]

Nakazawa MS, Keith B, and Simon MC (2016). Oxygen availability and metabolic adaptations. Nat Rev Cancer 16, 663–673. [PubMed: 27658636]

Parks SK, Chiche J, and Pouyssegur J (2013). Disrupting proton dynamics and energy metabolism for cancer therapy. Nat Rev Cancer 13, 611–623. [PubMed: 23969692]

Patra KC, Wang Q, Bhaskar PT, Miller L, Wang Z, Wheaton W, Chandel N, Laakso M, Muller WJ, Allen EL, et al. (2013). Hexokinase 2 is required for tumor initiation and maintenance and its systemic deletion is therapeutic in mouse models of cancer. Cancer Cell 24, 213–228. [PubMed: 23911236]

Pavlova NN, and Thompson CB (2016). The Emerging Hallmarks of Cancer Metabolism. Cell Metab 23, 27–47. [PubMed: 26771115]

Peng M, Yin N, Chhangawala S, Xu K, Leslie CS, and Li MO (2016). Aerobic glycolysis promotes T helper 1 cell differentiation through an epigenetic mechanism. Science 354, 481–484. [PubMed: 27708054]

Prezma T, Shteinfer A, Admoni L, Raviv Z, Sela I, Levi I, and Shoshan-Barmatz V (2013). VDAC1-based peptides: novel pro-apoptotic agents and potential therapeutics for B-cell chronic lymphocytic leukemia. Cell Death Dis 4, e809. [PubMed: 24052077]

Roberts DJ, and Miyamoto S (2015). Hexokinase II integrates energy metabolism and cellular protection: Akting on mitochondria and TORCing to autophagy. Cell Death Differ 22, 364. [PubMed: 25578149]

Rossignol R, Gilkerson R, Aggeler R, Yamagata K, Remington SJ, and Capaldi RA (2004). Energy substrate modulates mitochondrial structure and oxidative capacity in cancer cells. Cancer Res 64, 985–993. [PubMed: 14871829]

Schlee M, and Hartmann G (2016). Discriminating self from non-self in nucleic acid sensing. Nat Rev Immunol 16, 566–580. [PubMed: 27455396]

Schoggins JW, Wilson SJ, Panis M, Murphy MY, Jones CT, Bieniasz P, and Rice CM (2011). A diverse range of gene products are effectors of the type I interferon antiviral response. Nature 472, 481–485. [PubMed: 21478870]

Seth RB, Sun L, Ea CK, and Chen ZJ (2005). Identification and characterization of MAVS, a mitochondrial antiviral signaling protein that activates NF-kappaB and IRF 3. Cell 122, 669–682. [PubMed: 16125763]

Stark GR, and Darnell JE Jr. (2012). The JAK-STAT pathway at twenty. Immunity 36, 503–514. [PubMed: 22520844]

Tamura T, Yanai H, Savitsky D, and Taniguchi T (2008). The IRF family transcription factors in immunity and oncogenesis. Annu Rev Immunol 26, 535–584. [PubMed: 18303999]

Trinchieri G (2010). Type I interferon: friend or foe? J Exp Med 207, 2053–2063. [PubMed: 20837696]

Weinberg F, Hamanaka R, Wheaton WW, Weinberg S, Joseph J, Lopez M, Kalyanaraman B, Mutlu GM, Budinger GR, and Chandel NS (2010). Mitochondrial metabolism and ROS generation are essential for Kras-mediated tumorigenicity. Proc Natl Acad Sci U S A 107, 8788–8793. [PubMed: 20421486]

Wolf AJ, Reyes CN, Liang W, Becker C, Shimada K, Wheeler ML, Cho HC, Popescu NI, Coggeshall KM, Arditi M, et al. (2016). Hexokinase Is an Innate Immune Receptor for the Detection of Bacterial Peptidoglycan. Cell 166, 624–636. [PubMed: 27374331]

Xie H, Hanai J, Ren JG, Kats L, Burgess K, Bhargava P, Signoretti S, Billiard J, Duffy KJ, Grant A, et al. (2014). Targeting lactate dehydrogenase--a inhibits tumorigenesis and tumor progression in mouse models of lung cancer and impacts tumor-initiating cells. Cell Metab 19, 795–809. [PubMed: 24726384]

You F, Wang P, Yang L, Yang G, Zhao YO, Qian F, Walker W, Sutton R, Montgomery R, Lin R, et al. (2013). ELF4 is critical for induction of type I interferon and the host antiviral response. Nat Immunol 14, 1237–1246. [PubMed: 24185615]

Zeng W, Xu M, Liu S, Sun L, and Chen ZJ (2009). Key role of Ubc5 and lysine-63 polyubiquitination in viral activation of IRF3. Mol Cell 36, 315–325. [PubMed: 19854139]

Zhang J, Wang S, Jiang B, Huang L, Ji Z, Li X, Zhou H, Han A, Chen A, Wu Y, et al. (2017). c-Src phosphorylation and activation of hexokinase promotes tumorigenesis and metastasis. Nat Commun 8, 13732. [PubMed: 28054552]

Zhao W, Chang C, Cui Y, Zhao X, Yang J, Shen L, Zhou J, Hou Z, Zhang Z, Ye C, et al. (2014). Steroid receptor coactivator-3 regulates glucose metabolism in bladder cancer cells through coactivation of hypoxia inducible factor 1alpha. J Biol Chem 289, 11219–11229. [PubMed: 24584933]

Zhao Y, Wang A, Zou Y, Su N, Loscalzo J, and Yang Y (2016). In vivo monitoring of cellular energy metabolism using SoNar, a highly responsive sensor for NAD(+)/NADH redox state. Nat Protoc 11, 1345–1359. [PubMed: 27362337]

Zhong X, Tian S, Zhang X, Diao X, Dong F, Yang J, Li Z, Sun L, Wang L, He X, et al. (2017). CUE domain-containing protein 2 promotes the Warburg effect and tumorigenesis. EMBO Rep 18, 809–825. [PubMed: 28325773]

Zhu J, Zhang Y, Ghosh A, Cuevas RA, Forero A, Dhar J, Ibsen MS, Schmid-Burgk JL, Schmidt T, Ganapathiraju MK, et al. (2014). Antiviral activity of human OASL protein is mediated by enhancing signaling of the RIG-I RNA sensor. Immunity 40, 936–948. [PubMed: 24931123]

Zitvogel L, Galluzzi L, Kepp O, Smyth MJ, and Kroemer G (2015). Type I interferons in anticancer immunity. Nat Rev Immunol 15, 405–414. [PubMed: 26027717]

Highlights

- Lactate inhibits RLR-mediated interferon production.
- This regulation occurs through direct sensing of lactate by MAVS
- MAVS associates with hexokinase but this association is disrupted by RIG-I
- Targeting LDHA enhances type I IFN production and viral clearance

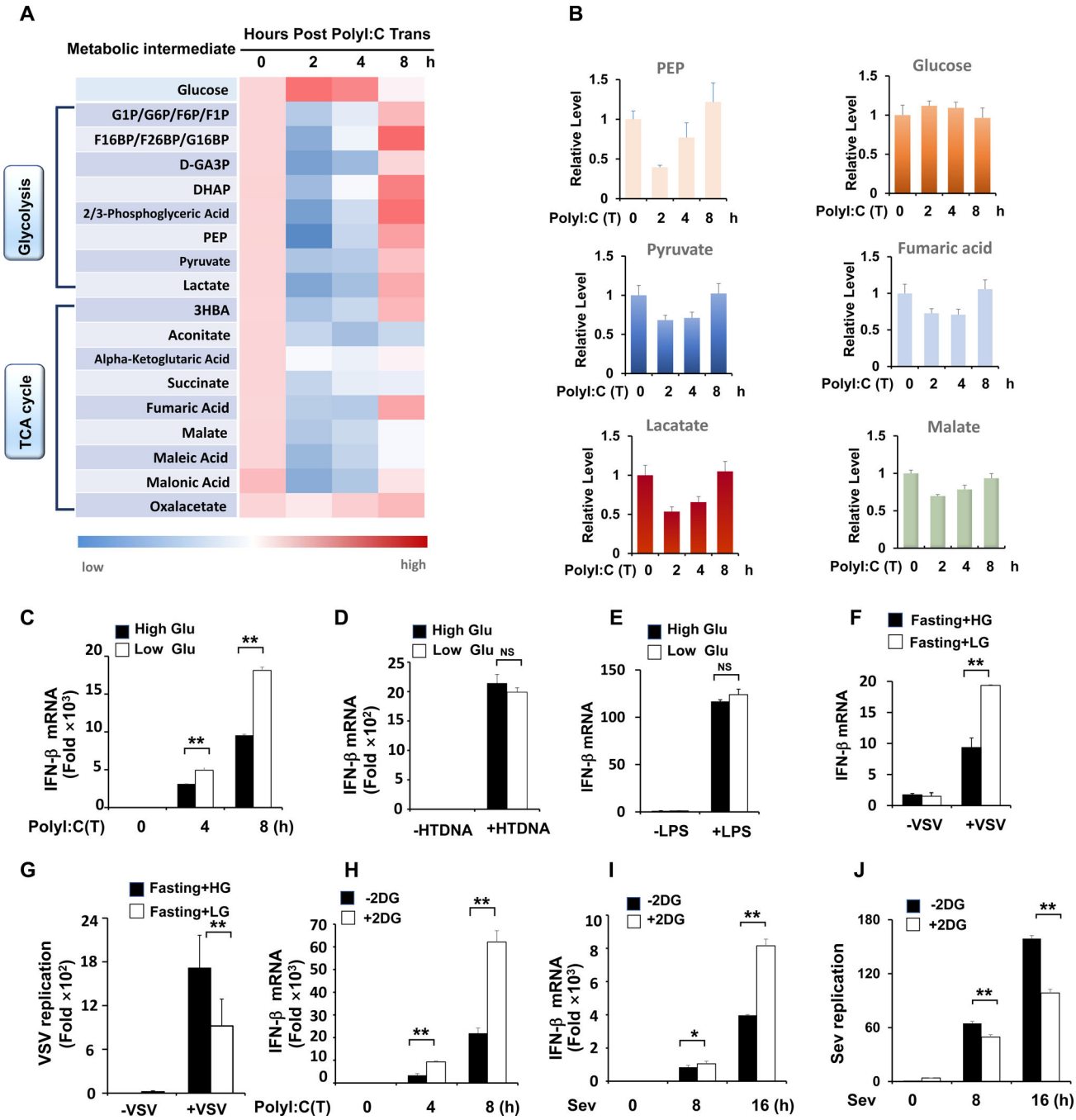

Figure 1. Downregulation of glucose metabolism promotes RLR induced type-I IFN production.

A, HEK293 cells were transfected with Poly(I:C) and harvested for metabolomics analysis. Shown is the heatmap for dynamic changes of metabolites in glycolysis or oxidative phosphorylation. **B**, Quantification analysis of some intermediates in glycolysis and TCA cycle. **C**, Q-PCR analysis of IFN-β mRNA expression in HEK293 cells cultured with high glucose (25 mM) or low glucose (5 mM) and transfected with Poly(I:C)(1μg/ml). **D and E**, Q-PCR analysis of IFN- β mRNA expression in THP1 cells transfected with HTDNA (1 μg/ml) or stimulated with LPS (50 ng/ml). **F and G**, Q-PCR analysis of IFN-β or VSV

mRNA expression from spleen tissue of mice fasted overnight and then treated with high glucose (1.5 g/kg) or low glucose (0.2 g/kg). **H–J**, Q-PCR analysis of IFN- β and Sendai viral specific gene expression in HEK293 cells pretreated with or without 2DG (2mM) and then transfected with Poly(I:C) (1 μg/ml) or infected with Sendai virus for indicated hours. Data are means±SD. * $p < 0.05$, ** $p < 0.01$. **See also** Figure S1.

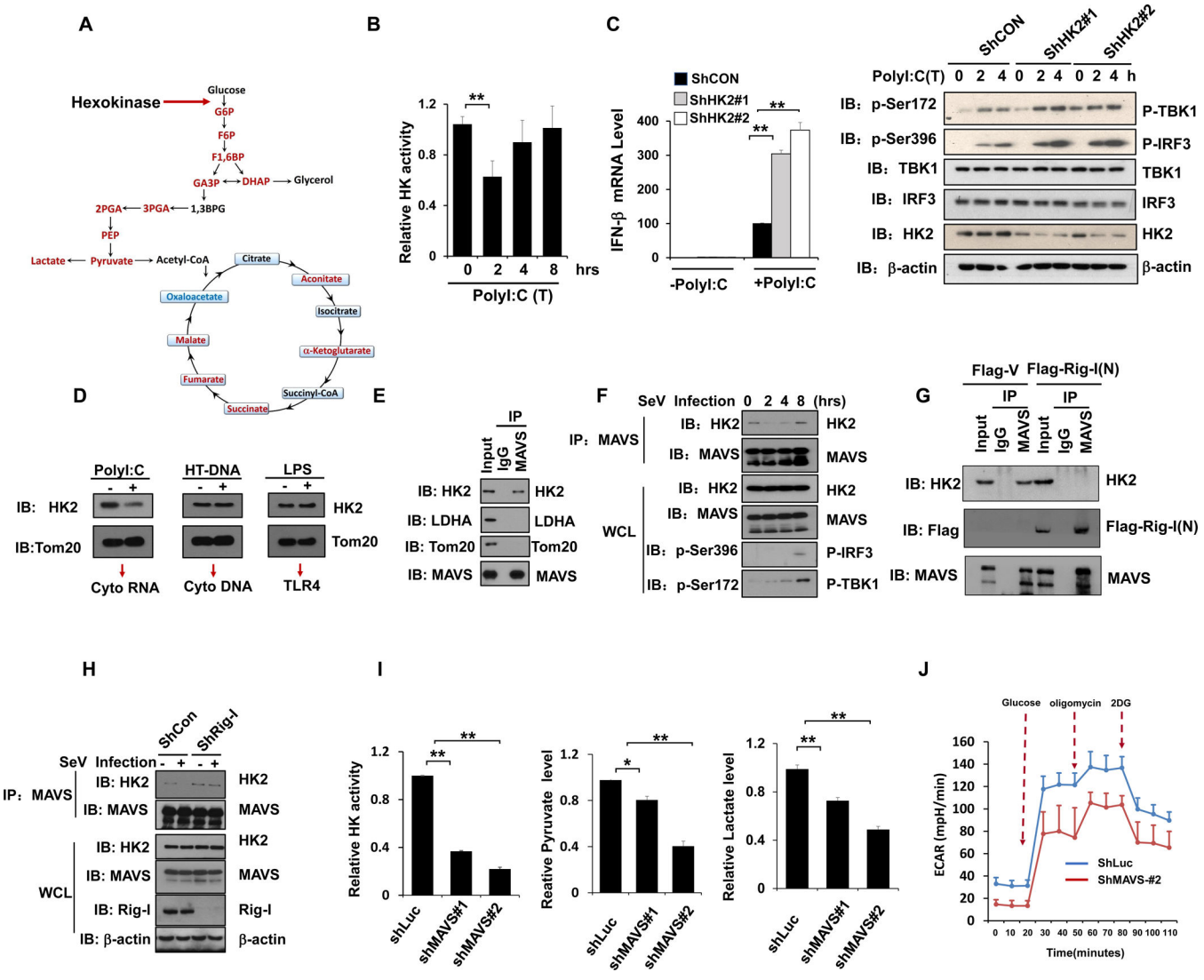

Figure 2. Mitochondria hexokinase activity is maintained by MAVS and inactivated during RLR activation.

A, Scheme of selected reactions in glucose metabolic pathway. **B**, Analysis of hexokinase (HK) activity in purified mitochondria isolated from HEK293 cells transfected with poly(I:C). **C**, Q-PCR analysis of IFN-β mRNA expression in control or HK2 knockdown Hep3B cells transfected with or without Poly(I:C) (left panel). Immunoblot analysis of Hep3B cells with control or HK2 knockdown (right panel). **D**, Immunoblot analysis of HK2 level in the mitochondria fraction from THP1 cells transfected with Poly(I:C), HTDNA or stimulated with LPS. Tom20 was used as a mitochondria marker. **E-F**, Whole cell lysis of HEK293 cells infected with or without Sev were collected for immunoprecipitation (IP) with IgG or MAVS antibody, followed by Immunoblot (IB) analysis. **G**, HEK293 cells transfected with Flag-V or Flag-RIG-I(N) were immunoprecipitated with indicated antibodies and IP complexes were analyzed by IB analysis. **H**, HEK293 cells with control or RIG-I knockdown were infected with Sev for 4 hours and whole cell lysis were collected for IP with MAVS antibody, followed by IB analysis for indicated proteins. **I and J**,

Measurement of mitochondria hexokinase activity, total pyruvate level, lactate level and ECAR in Hep3B cells with control or MAVS knockdown. Data are means±SD. * $p < 0.05$, **$p < 0.01$. **See also** Figure S2.

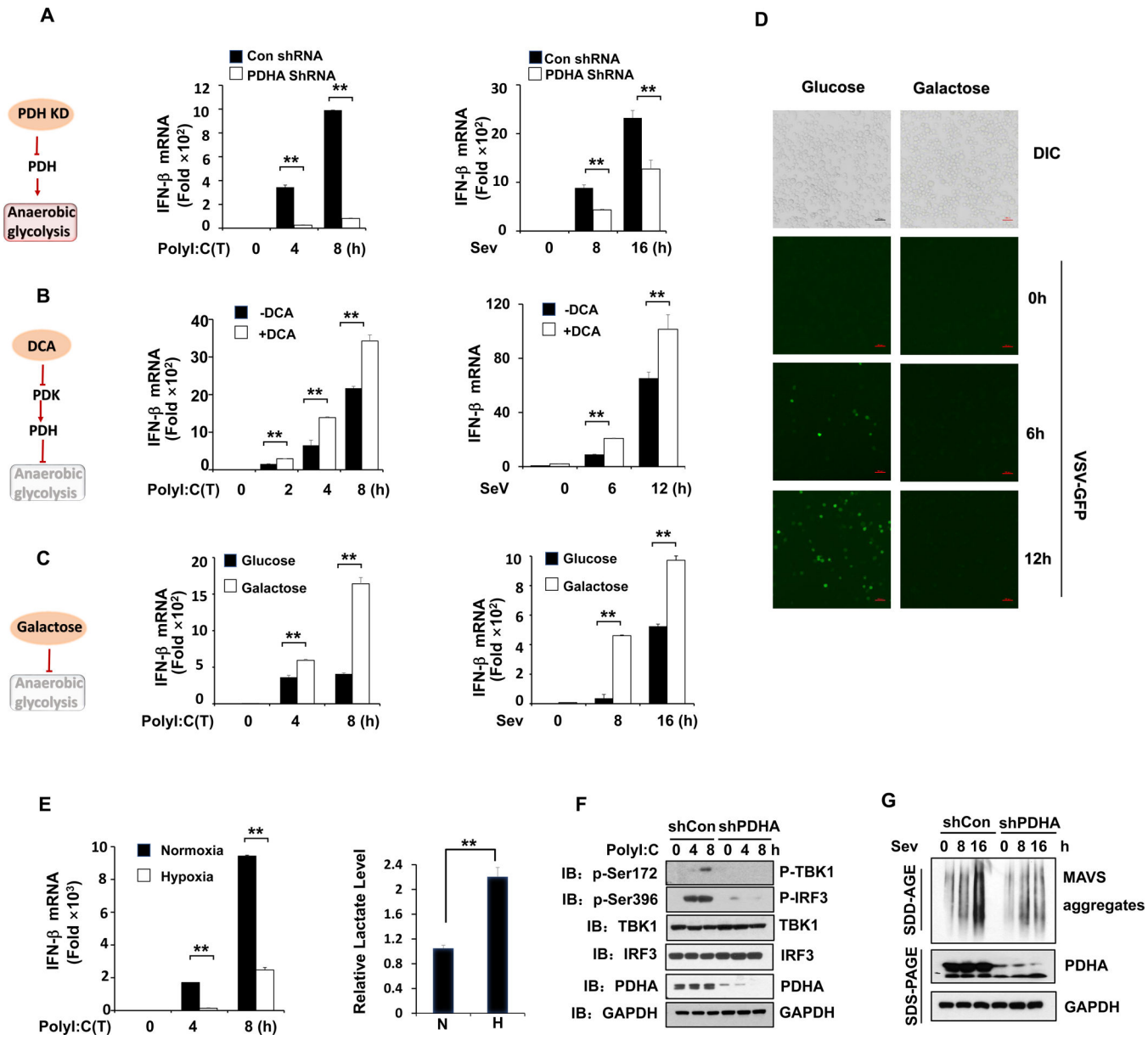

Figure 3. Anaerobic glycolysis inhibits RLR triggered MAVS-TBK1-IRF3 activation and type-I IFN production.

A–B, Q-PCR analysis of IFN-β mRNA expression in HEK293 cells with or without PDHA knockdown (A), or pretreated with or without DCA (10 mM) (B) and then transfected with Poly(I:C) (left panel) or infected with Sendai virus (right panel) for indicated times. **C**, Q-PCR analysis of IFN- β mRNA expression in immortalized bone marrow macrophage (iBMM) cells cultured in mediums containing glucose (25 mM) or galactose (25 mM) and then transfected with Poly(I:C) (left panel) or infected with Sendai virus (right panel) for indicated times. **D**, Microscopic images of VSV-GFP-infected iBMM cells pre-cultured in the same conditions as in C and then infected with VSV-GFP (MOI=0.1) as indicated times. Scale bar, 100 μm. **E**, Q-PCR analysis of IFN-β mRNA expression (left panel) and measurement of lactate secretion (right panel) in HEK293 cells exposed to normoxia (20%

O_2) or hypoxia (1% O_2) and transfected with Poly(I:C). **F**, Immunoblot analysis of HEK293 cells with control or PDHA knockdown and transfected with Poly(I:C) for indicated times. **G**, Immunoblot analysis of HEK293 cells with control or PDHA knockdown. Cell mitochondria were isolated for SDD-AGE (upper panel) and whole cell lysates were used for SDS-PAGE (lower panel). Data are means±SD. **p < 0.01. **See also** Figure S3.

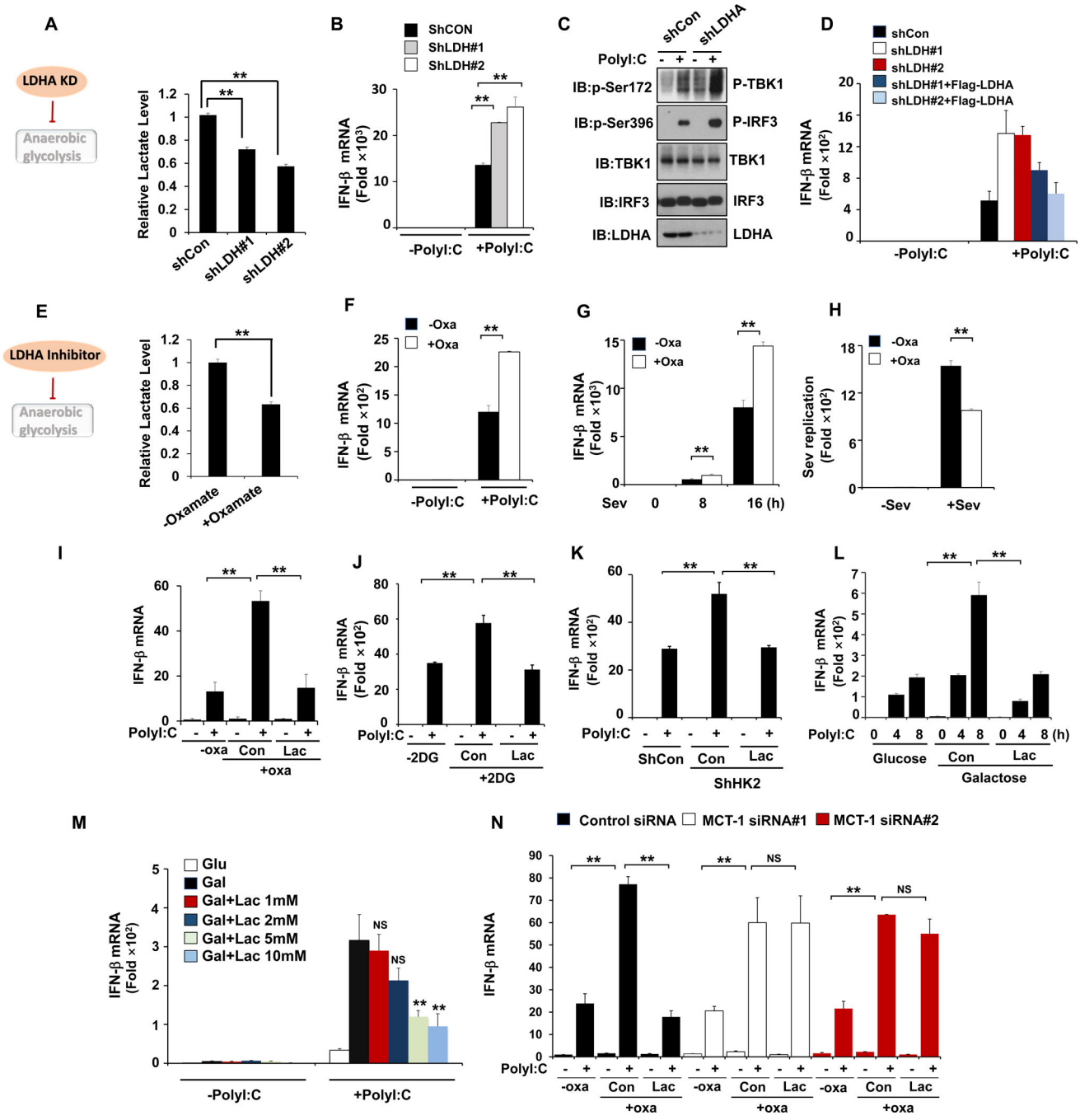

Figure 4. LDHA-associated lactate negatively regulates RLR signaling.

A–C, Measurement of lactate secretion (A), IFN-β mRNA expression (B) or protein levels (C) in Hep3B cells with control or LDHA knockdown and transfected with Poly (I:C) for 4 hours. **D**, Q-PCR analysis of IFN-β mRNA expression in Hep3B cells infected with control or LDHA shRNA along with or without Flag-LDHA expression and then transfected with Poly (I:C). **E**, Measurement of lactate secretion in HEK293 cells pretreated with or without Sodium Oxamate (20 mM) overnight. **F-H**, Q-PCR analysis of IFN- μ or Sev mRNA expression in HEK293 cells treated with or without sodium oxamate (20 mM) overnight and

then transfected with Poly(I:C) for 2 hours or infected with Sev as indicated. **I and J**, Q-PCR analysis of IFN-β mRNA expression in Hep3B cells pretreated with or without sodium oxamate (20 mM) or 2-DG (2mM) and then added with or without Lactate (10 mM) before transfecting with Poly(I:C). **K**, Q-PCR analysis of IFN-β mRNA expression in Hep3B cells infected with control or HK2 shRNA and then added with or without Lactate (10 mM) before transfecting with Poly(I:C). **L–M**, Q-PCR analysis of IFN-β mRNA expression in iBMM cells cultured in mediums containing glucose (25 mM) or galactose (25 mM) and then added with or without Lactate before transfecting with Poly(I:C). **N**, Q-PCR analysis of IFN-β mRNA expression in Hep3B cells with control or MCT1 knockdown and then treated with or without sodium oxamate (20mM) overnight before lactate addition (10 mM) and poly(I:C) transfection. Data are means±SD. **p < 0.01. **See also** Figure S4 **and** S5.

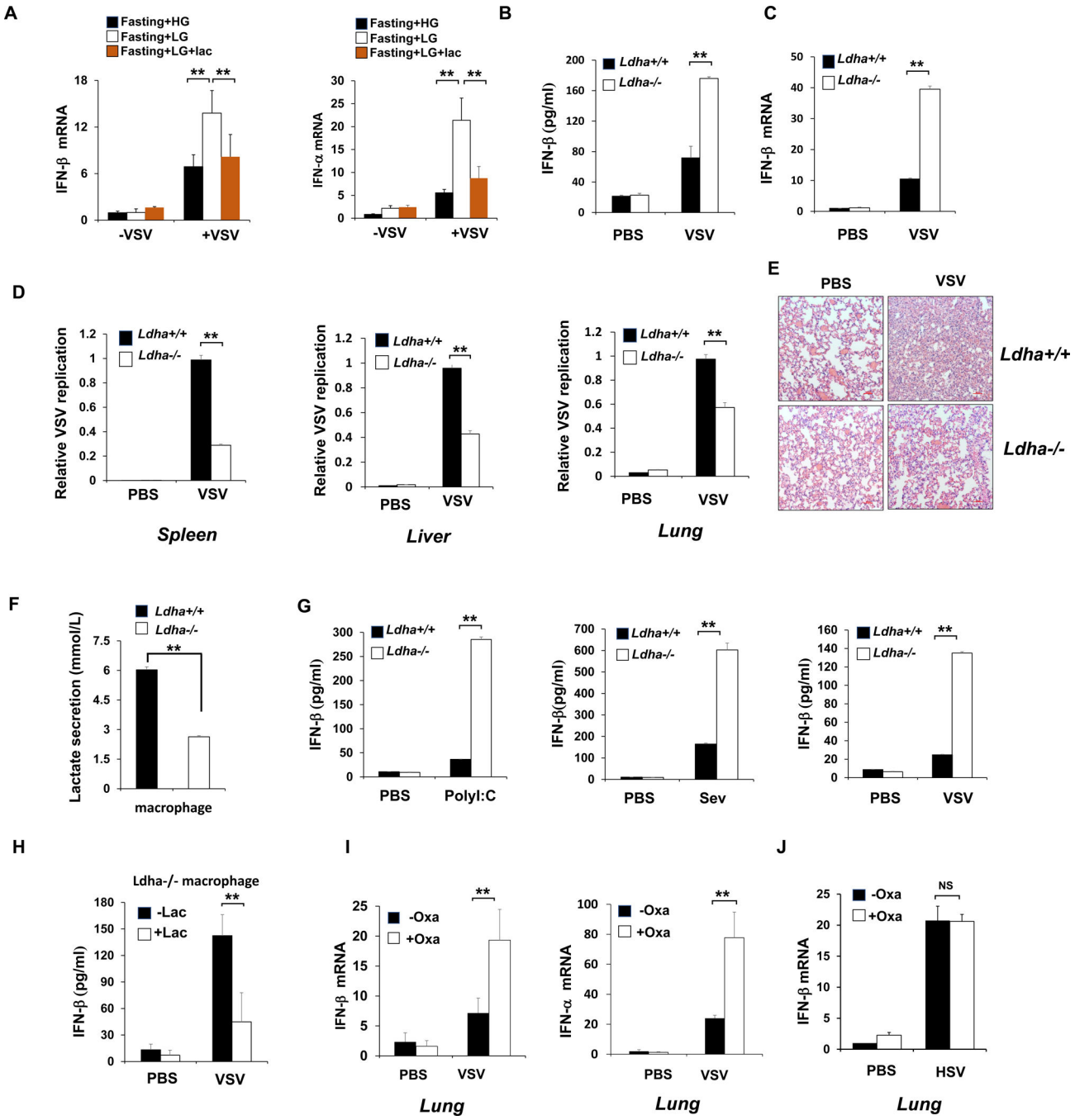

Figure 5. LDHA-associated lactate inhibits RLR signaling *in vivo*.

A, Q-PCR analysis of IFN-β and IFN-α expression in lung from mice fasted overnight and then treated with high glucose (1.5 g/kg) or low glucose (0.2 g/kg) with or without following injection of sodium lactate (1 g/kg) and infected with VSV (2×10^7 pfu/g). **B**, ELISA analysis of IFN- β in sera of *Ldha*$^{+/+}$ and *Ldha*$^{-/-}$ mice intraperitoneal injected with VSV (2×10^7 pfu/g). **C and D**, Q-PCR analysis of IFN- β expression in spleen (C) and VSV replication in different organs (D) from *Ldha*$^{+/+}$ and *Ldha*$^{-/-}$ mice infected with VSV. **E**, Hematoxylin and eosin (HE) staining of lung sections in *Ldha*$^{+/+}$ and *Ldha*$^{-/-}$ mice

described in D. Scale bar, 100 mm. **F and G**, Analysis of lactate secretion (F) and IFN-β production (G) in supernatants of peritoneal macrophages generated from *Ldha*$^{+/+}$ and *Ldha*$^{-/-}$ mice and treated with Poly(I:C) transfection, Sev or VSV infection. **H**, ELISA analysis of IFN-β production in supernatants of peritoneal macrophages generated from *Ldha*$^{-/-}$ mice and then added with or without lactate (10 mM) before VSV infection. **I**, Q-PCR analysis of type-I IFN expression in lung from mice injected with or without sodium oxamate (750 mg/kg) and then challenged by VSV (2×10^7 pfu/g). **J**, Q-PCR analysis of IFN-β mRNA expression in lung tissue from mice injected with or without sodium oxamate and infected with HSV. Data are means±SD. **p < 0.01. **See also** Figure S6.

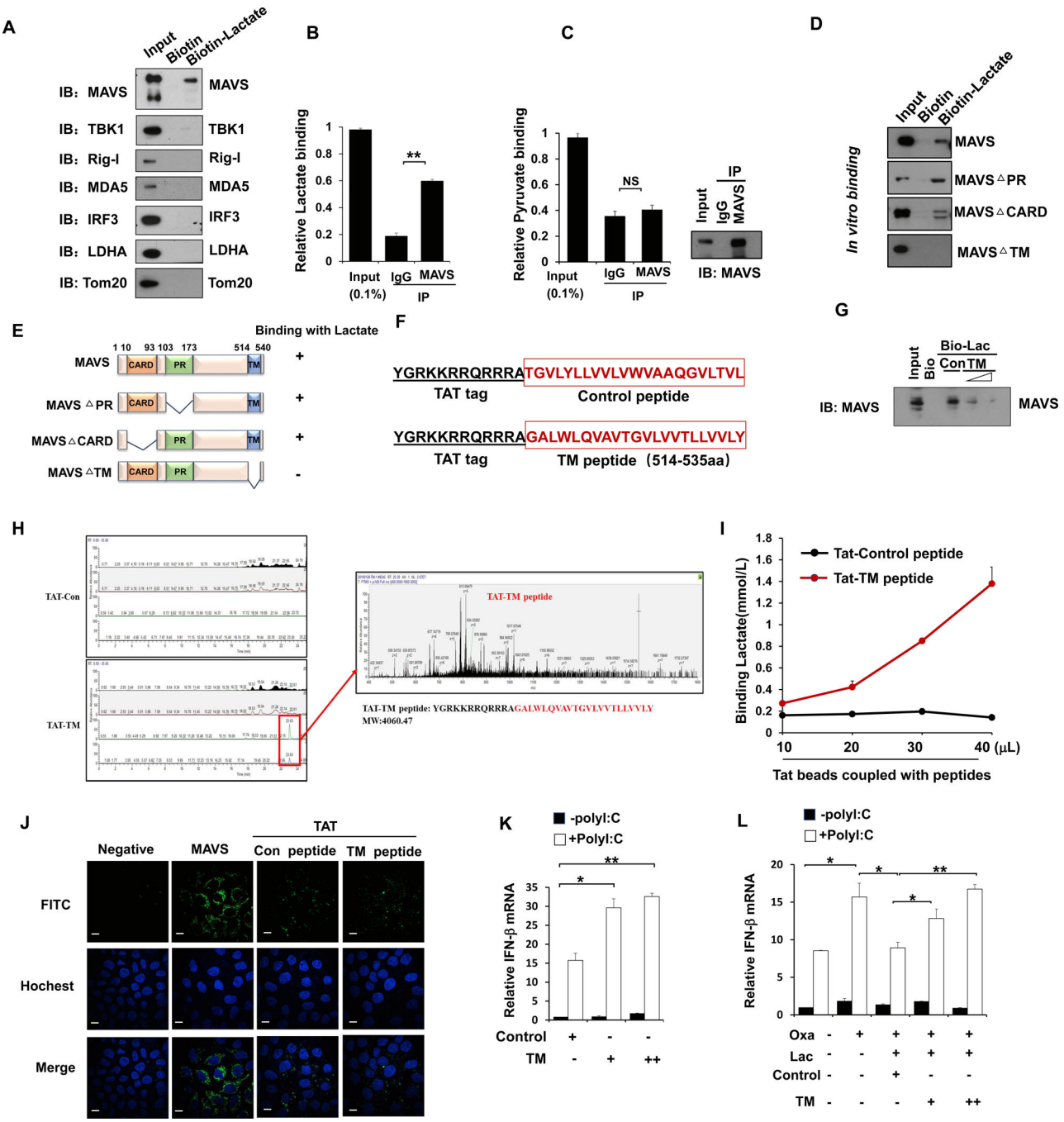

Figure 6. LDHA-associated lactate negatively regulates RLR activation by targeting MAVS.

A, Immunoblot analysis of binding complexes isolated from HEK293 cell extracts incubated with biotin-labeled lactate or biotin control. **B and C**, Fluorescence analysis of lactate or pyruvate binding in complexes immunoprecipitated (IP) by IgG or anti-MAVS antibody from HEK293 cells. **D and E**, Immunoblot analysis of *in vitro* mapping assays among biotin-labeled lactate and various MAVS truncated protein translated *in vitro* by the TNT system. **F**, Schematic representation of the sequence for control or TM peptide of MAVS with TAT tag in N-terminal region. **G**, Immunoblot analysis of *in vitro* pulldown assays by

incubating biotin-labeled lactate or biotin control with MAVS protein translated *in vitro* by the TNT system along with control or TM peptide. **H**, TM peptides identified by Mass Spectrometry through *in vitro* pulldown assay. **I**. Analysis of lactate binding with different doses of Tat-control or Tat-TM peptide. **J**, Immunofluorescence analysis of cellular localization of control or TM peptide in HeLa cells pretreated with each peptides, stained with MAVS or TAT antibody and imaged by confocal microscopy. Scale bar, 10 mm. **K**, Q-PCR analysis of IFN-β expression in Hep3B cells treated by control or TM peptide of MAVS and transfected with Poly(I:C). **L**, Q-PCR analysis of IFN-β expression in Hep3B cells pretreated with or without sodium oxamate overnight, then incubated with control or TM peptide of MAVS for 2 hours and addition of lactate, followed by transfection of Poly(I:C). Data are means±SD. *$p < 0.05$, **$p < 0.01$. **See also** Figure S7.

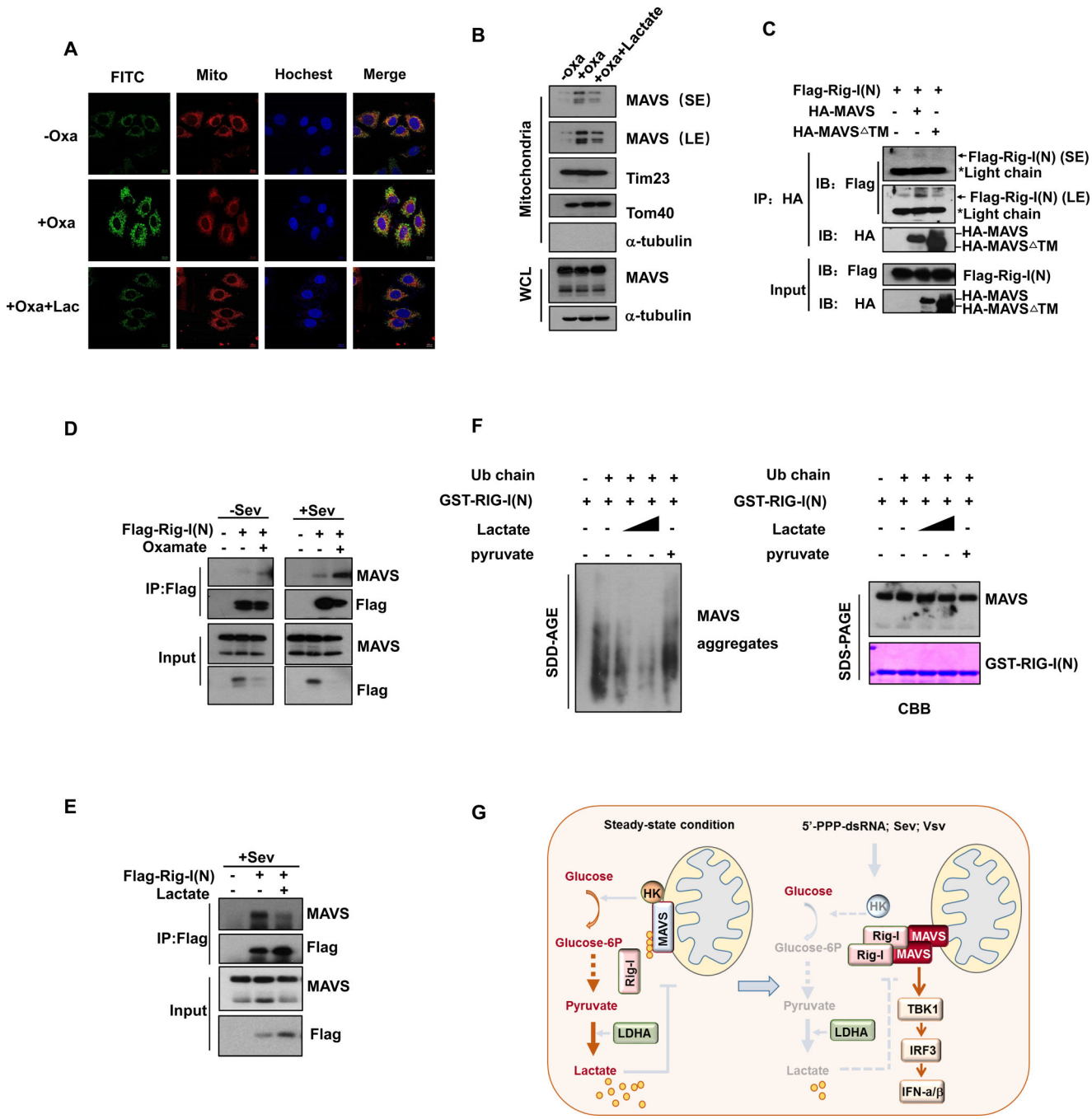

Figure 7. Lactate inhibits RIG-I/MAVS association and MAVS aggregation.

A, Immunofluorescence analysis of cellular localization of MAVS in Hep3B cells pretreated with or without Oxamate and added with lactate. Scale bar, 10mm. **B**, Immunoblot analysis of mitochondria fraction isolated from HEK293 cells treated as indicated. **C-E**, Cell lysates from HEK293 cells transfected or treated as indicated were immunoprecipitated with antibodies indicated, and IP complexes were analyzed by immunoblot analysis. **F**, Immunoblot analysis of *in vitro* MAVS aggregation. GST-RIG-I(N) was incubated with K63-Ub4 and then with mitochondria isolated from HEK293 cells preincubated with or

without lactate (5 mM,10 mM) or pyruvate, followed by analysis of mitochondria extracts using SDD-AGE (left panel) and SDS-PAGE (right panel). GST-RIG-(N) was shown by Coomassie blue staining (CBB). **G**, Illustration of how glycolysis-derived lactate inhibits RLR signaling by targeting MAVS.

KEY RESOURCES TABLE

REAGENT or RESOURCE	SOURCE	IDENTIFIER
Antibodies		
Mouse monoclonal anti-MAVS(E-3)	Santa Cruz Biotechnology	Cat# sc-166583; RRID:AB_2012300
Mouse monoclonal anti-HK2(B-8)	Santa Cruz Biotechnology	Cat# sc-374091; RRID:AB_10917915
Mouse monoclonal anti-β-Actin(C4)	Santa Cruz Biotechnology	Cat# sc-47778; RRID: AB_626632
Mouse monoclonal anti-c-Myc(9E10)	Santa Cruz Biotechnology	Cat# sc-40; AB_627268
Rabbit polyclonal anti-HA-probe	Santa Cruz Biotechnology	Cat# sc-805; RRID: AB_631618
Rabbit monoclonal anti-Rig-l(D14G6)	Cell Signaling Technology	Cat# 3743; RRID:AB_2269233
Rabbit monoclonal anti-TBK1(D1B4)	Cell Signaling Technology	Cat# 3504; RRID:AB_2255663
Rabbit monoclonal anti-IRF3(D6l4C)	Cell Signaling Technology	Cat# 11904; RRID:AB_2722521
Rabbit monoclonal anti-TBK1(phosS172) (D52C2)	Cell Signaling Technology	Cat# 5483; RRID:AB_10693472
Rabbit monoclonal anti-IRF3(phosS396) (4D4G)	Cell Signaling Technology	Cat# 4947; RRID:AB_823547
Rabbit monoclonal anti-PDHA(C54G1)	Cell Signaling Technology	Cat# 3205; RRID:AB_2162926
Rabbit monoclonal anti-MDA5(D74E4)	Cell Signaling Technology	Cat# 5321; RRID:AB_10694490
Rabbit polyclonal anti-MAVS	Cell Signaling Technology	Cat# 3993; RRID:AB_823565
Rabbit polyclonal anti-LDHA	Cell Signaling Technology	Cat# 2012; RRID:AB_2137173
Mouse monoclonal anti-HIV-TAT(N3)	Abcam	Cat# ab63957; RRID:AB_1139536
Bacterial and Virus Strains		
VSV-GFP	Prof. Zhijian J. Chen (UT Southwestern Medical Center, USA).	N/A
HSV-1	Prof. Jiahuai Han (Xiamen U. China)	N/A
SEV	ATCC	Cat# VR907
Chemicals, Peptides, and Recombinant Proteins		
D-(+)-Glucose	Sigma-Aldrich	Cat# G7021
D-(+)-Galactose	Sigma-Aldrich	Cat# G0750
L(+)-Lactic acid	Sigma-Aldrich	Cat# L1750
Sodium L-lactate	Sigma-Aldrich	Cat# L7022
Sodium Oxamate	Sigma-Aldrich	Cat# 02751
2-Deoxy-D-glucose(2-DG)	Sigma-Aldrich	Cat# D8375
Sodium dichloroacetate(DCA)	Sigma-Aldrich	Cat# 347795
UK5099	Sigma-Aldrich	Cat# PZ0160
Poly(l:C)	Sigma-Aldrich	Cat# P1530
HT-DNA	Sigma-Aldrich	Cat# D6898
Tamoxifen	Sigma-Aldrich	Cat# 10540-29-1
TRIzol	Thermo Fisher Scientific	Cat# 15596018
Dynabeads MyOne Streptavidin T1	Thermo Fisher Scientific	Cat# 65601
Human Tetra Ubiquitin/Ub4 WT Chains (K63linked)	R&D	Cat# UC310B
Con-peptide	This paper	N/A
TM-peptide	This paper	N/A

REAGENT or RESOURCE	SOURCE	IDENTIFIER
VDAC competitive peptide	(Prezma et al., 2013)	N/A
Critical Commercial Assays		
Mouse IFN-β ELISA kit	Thermo Fisher	Cat# 424001
Hexokinase Colorimetric assay kit	Biovision	Cat# K789–100
Lactate Colorimetric/Fluorometric assay kit	Biovision	Cat# K607–100
Mitochondria isolation kit	Thermo Fisher	Cat# 89874
Experimental Models: Cell Lines		
Human: HEK293	ATCC	Cat# CRL-11268
Human: THP-1	ATCC	Cat# TIB-202
Human: Hep3B	ATCC	Cat# HB-8064
Mouse: Raw264.7	ATCC	ATCC® TIB-71™
Mouse: iBMM	Prof. Feng Shao (National Institute of Biological Sciences, China)	N/A
Mouse: primary peritonea macrophages	This paper	N/A
Experimental Models: Organisms/Strains		
Mouse: Cre^{tm}-$LDHA^{fl/fl}$ C57BL/6J	(Xie et al., 2014)	N/A
Oligonucleotides		
siRNA: human *MCT1*-#1	RiboBio	Cat# stB0007914A
siRNA: human *MCT1*-#2	RiboBio	Cat# stB0007914B
siRNA: human *PDHA*	Thermo Fisher	Cat# 4427038
ShRNA: human *HK2*-#1	Sigma-Aldrich	Cat# TRCN0000037670
ShRNA: human *HK2*-#2	Sigma-Aldrich	Cat# TRCN0000195582
ShRNA:human *MAVS*-#1	Sigma-Aldrich	Cat# TRCN0000236029
ShRNA: human *MAVS*-#2	Sigma-Aldrich	Cat# TRCN0000236030
ShRNA: human *Rig-I*	Sigma-Aldrich	Cat# TRCN0000153712
ShRNA: human *PDHA*	Sigma-Aldrich	Cat# TRCN0000028630
ShRNA: human *LDHA*#1	Sigma-Aldrich	Cat# TRCN0000164922
ShRNA: human *LDHA*#2	Sigma-Aldrich	Cat# TRCN0000026541
qPCR pimers, see Table S1	This paper	N/A
Recombinant DNA		
PCDNA3-MAVS	Prof. Zhijian J. Chen (UT Southwestern Medical Center, USA).	N/A
pEF-BOS-Flag-RIG-l	Prof. Zhijian J. Chen (UT Southwestern Medical Center, USA).	N/A
Human *HK2* cDNA Construct	Prof. Qinxi Li(Xiamen U. China)(Zhang et al.,2017)	N/A
Human *LDHA* cDNA Construct	Prof. Ping Gao(Xiamen U. China)(Zhong et al.,2017)	N/A
Human *VDAC* cDNA Construct	Prof. Hui Zhong (Molecular Genetics Department Beijing Institute of Biotechnology, China)(Guanetal., 2013)	N/A